Anomalous Transport Scaling in the DIII-D Tokamak Matched by Supercomputer Simulation

J. Candy* and R. E. Waltz
General Atomics, P.O. Box 85608, San Diego, California 92186-5608, USA
(Received 5 December 2002; published 23 July 2003)

Gyrokinetic simulation of tokamak transport has evolved sufficiently to allow direct comparison of numerical results with experimental data. It is to be emphasized that only with the simultaneous inclusion of many distinct and complex effects can this comparison realistically be made. Until now, numerical studies of tokamak microturbulence have been restricted to either (a) flux tubes or (b) electrostatic fluctuations. Using a newly developed global electromagnetic solver, we have been able to recover via direct simulation the Bohm-like scaling observed in DIII-D L-mode discharges. We also match, well within experimental uncertainty, the measured energy diffusivities.

DOI: 10.1103/PhysRevLett.91.045001 PACS numbers: 52.55.Dy, 52.30.Gz, 52.35.Qz, 52.65.Tt

Over the last decade, gyrokinetic simulation of tokamak transport has matured sufficiently to allow direct, *quantitative* comparison of numerical results with experimental data. Only with the simultaneous inclusion of many distinct and complex effects can this comparison realistically be made. We believe the crucial physics components for comprehensive gyrokinetic simulation are the following: (1) nonlinear gyrokinetic ions and electrons (both trapped and passing populations), (2) radial profile variation with sheared equilibrium $\mathbf{E} \times \mathbf{B}$ rotation and parallel velocity shear (i.e., global simulation), (3) shaped plasma geometry (elongation, triangularity, etc.), (4) electron pitch-angle scattering, and (5) electromagnetic fluctuations, $\delta A_{\parallel}$, at finite plasma β. Note that item (2) refers to what are customarily called "finite-ρ_*" effects. Here, $\rho_* \doteq \rho_s/a$, with ρ_s the ion-sound Larmor radius and a the plasma minor radius.

In the high-confinement mode (H-mode) of tokamak operation, diffusivities are typically found to exhibit gyroBohm scaling: $\chi = C\chi_{GB}$ [1]. Here, C is a coefficient which depends on dimensionless parameters, $\chi_{GB} \doteq \rho_*\chi_B$ is the gyroBohm scaling factor, $\chi_B \doteq \rho_s c_s$ is the Bohm scaling factor, and $c_s = \sqrt{T_e/m_i}$ is the sound speed. Although gyroBohm scaling is intrinsic to local gyrokinetic simulations, low confinement (L-mode) discharges often show scaling between Bohm and gyroBohm. This observation suggests that global simulation is an inevitable requirement to understand transport in existing tokamaks. With the goal of making fully realistic calculations of turbulent transport, we developed an Eulerian gyrokinetic-Maxwell code. This code, GYRO [2], was designed from the outset to include all the physics components enumerated in the introduction.

Historically, the algorithm of choice for global nonlinear gyrokinetic simulation has been the gyrokinetic particle-in-cell (GK-PIC) method [3–5]. Yet, attempts to describe electromagnetic fluctuations with the GK-PIC method have met with numerous obstacles. Experience has shown that the kinetic ballooning mode (KBM) branch which arises at finite β is difficult to describe gyrokinetically — because two terms in the Ampère equation, which are small in the limit $\beta_e \to 0$, are large and must cancel exactly when $\beta_e(m_i/m_e) > 1$. To remedy this problem, special discretization techniques are required. These were first developed for use in flux-tube [6] and global [2] Eulerian codes, and more recently for flux-tube PIC codes [7].

For years now, a prominent feature of global GK-PIC simulations has been worse-than-gyroBohm scaling over a wide range of parameters [3,8]. Although attempts were made to recover gyroBohm scaling from global GK-PIC simulations in the limit $\rho_* \to 0$, no physically clear demonstration of the transition was ever shown. Using GYRO(with adiabatic electrons), we were able to clearly demonstrate the transition from gyroBohm to Bohm (and worse) scaling via finite-ρ_* effects due to profile variation [9]. Subsequently, global PIC simulations — without profile or gyroradius variation (that is, flat T_i and dT_i/dr) — reported by Lin and co-workers [5] showed a gradual transition from worse-than-Bohm to gyroBohm scaling as $1/\rho_*$ varied between 125 and 1000. For the parameters used, it was our *a priori* expectation (subsequently confirmed by simulation) that gyroBohm scaling ought to be obtained for $1/\rho_* > 200$. Thus, the mechanism through which gyroBohm scaling is broken in these GK-PIC simulations remains unexplained.

GYRO uses a variety of novel numerical methods not found in other solvers. The kinetic equation, for example, is not differenced in poloidal angle, but rather in *orbit time* using a third-order upwind scheme. This approach removes the singularity due to trapped particle bounce points thereby minimizing the required number of grid points in the poloidal direction. The toroidal direction is spectral, with fluctuating quantities expanded as $f = \sum_n \exp[-in(\varphi - q\theta)] f_n$. Here, φ and θ are the toroidal and poloidal angles. The Maxwell equations (diagonal in n) are solved with a Galerkin finite-element scheme. The associated matrix problem is sparse, and solution time

scales linearly with the number of radial grid points and poloidal finite elements. Radial derivatives and gyroaverages use high-order radial stencils, and nonlinear terms are treated with a conservative, nondissipative Arakawa-like discretization scheme. For the time advance we use a recently developed second-order implicit-explicit Runge-Kutta scheme [10]. This treats the linear electron advection implicitly (removing the dominant stiff terms in the gyrokinetic-Maxwell system), is strong-stability-preserving in the stiff limit, and causes no performance degradation in comparison with previous fully explicit schemes. Multilayer radial boundary conditions are used to gradually and self-consistently attenuate the distributions and fields outside of the simulation domain. *These were carefully designed so that, in the absence of profile variation, diffusivities match those obtained with flux tubes.* Finally, electron collisions (pitch-angle scattering) are treated in a semi-implicit fashion using operator splitting — with no viscous Courant limit on the time step.

The focus of this Letter is to report a series of gyrokinetic simulations with the level of physical realism indicated by items (1)–(5). *These simulations reproduce not only the Bohm-like ρ_* scaling observed in DIII-D L-mode discharges* [11], *but also match the actual values of the experimentally inferred transport coefficients within error bars.* This is the first study in which comprehensive global gyrokinetic calculations have included enough physics to be meaningfully compared with experiments. Previous comprehensive flux-tube studies [12], which neglected the profile and $\mathbf{E} \times \mathbf{B}$ shearing effects, have tended to more strongly overestimate the experimental levels of transport in DIII-D plasmas.

Here we describe simulations of DIII-D L-mode discharges 101381 and 101391 [11]. These are dimensionally similar shots differing only in ρ_* which give nearly identical *local* linear gyrokinetic growth rates over a wide profile range. Obtaining this well-matched pair is clearly a remarkable experimental achievement. At the arbitrarily chosen *reference radius,* $r_0/a = 0.6$, these discharges are characterized by two different values of ρ_* as summarized in Table I. These discharges have a χ_i ratio (0.55) which is slightly worse than Bohm (0.65).

Our explicit goal is to compute selected transport coefficients at the reference radius — in particular, the energy diffusivity:

$$\chi(r) = \left(-N\frac{dT}{dr}\right)^{-1} \int d^3v (mv^2/2) \langle \delta v_r \cdot \overline{\delta} f \rangle, \quad (1)$$

where $\langle a \cdot b \rangle = 2\{\sum_{n>0} \mathrm{Re}[(a^*)_n b_n]\}_{t\theta}$. Above, $\overline{\delta} f$ is the gyroaveraged gyrocenter distribution, δv_r is the radial component of the fluctuating $\mathbf{E} \times \mathbf{B}$ drift velocity, N and T are the equilibrium density and temperature, and $\{\}_{t\theta}$ indicates an average over time and flux surface. Although GYRO also computes the particle and momentum diffusivities as well as electron-ion energy exchanges, we discuss only χ in this Letter. We have found that it is typically not necessary to simulate the entire radial

TABLE I. Summary of key parameters at $r/a = 0.6$. B_T is the toroidal field. Other parameters are defined in the text.

Quantity	101381	101391	Ratio
B_T	1.05 T	2.1 T	0.5
$\chi_{\mathrm{GB}} = \rho_s^2 c_s/a$	1.93 m/s^2	1.02 m/s^2	$(0.53)^{-1}$
ρ_*	0.004	0.0026	$(0.65)^{-1}$
$\chi_i^{\mathrm{exp}}/\chi_{\mathrm{GB}}$	1.2	2.2	0.55

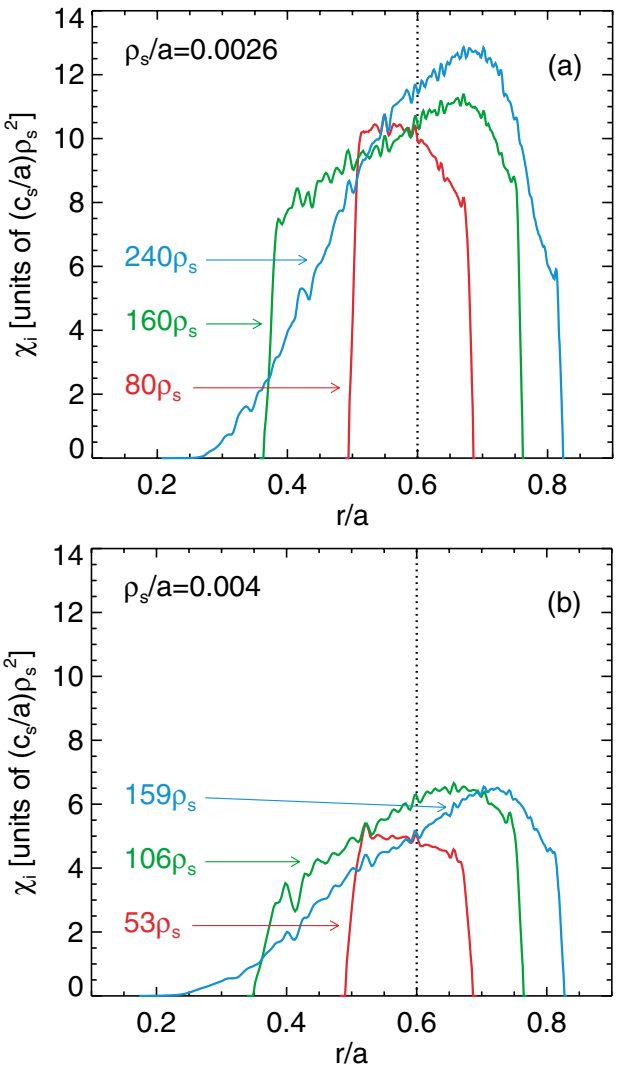

FIG. 1 (color online). Box-size study showing time-averaged χ_i profiles for $\rho_* = 0.0026$ (a) and $\rho_* = 0.004$ (b). These simulations include all physics effects, but with reduced mass ratio ($m_i/m_e = 400$). At the reference point, $r/a = 0.6$, the small-box simulation is a good approximation to the full-domain calculation, but at substantially reduced computational expense.

domain to get a good estimate of the transport at a particular r_0. Figure 1 shows a scan of box size for both the 101381 and 101391 cases (carried out at reduced mass ratio: $m_i/m_e = 400$). Note that the results are roughly in the Bohm ratio and the profiles of χ_i have the characteristic increase with radius for the larger boxes. The quality of the overlap at r_0 is sufficiently good that we decided to carry out all subsequent simulations with the smallest indicated boxes for substantially reduced computational expense. A critical adaptive source algorithm is used in all simulations to ensure that there is no turbulent modification to the equilibrium density and temperature profiles [9]. All simulations used 128 velocities (eight energies, eight pitch angles, two signs of velocity), 16 complex toroidal harmonics spanning $0.0 \leq k_\theta \rho_s \leq 0.9$, 1.8 radial grid points per local ion gyroradius (for example, 144 grid points for an $80\rho_s$ box) with 5-point and 15-point stencils for radial derivatives and gyroaverages, respectively. High-k electron temperature gradient modes are omitted. With the exception of the box-size scans of Fig. 1, all simulations use real mass ratio ($m_i/m_e = 3600$). We also use experimental equilibria, temperature, density, and E_r profiles in all cases—an absolute necessity for both linear and nonlinear comparison with DIII-D discharges. With regard to additional physics, subsequent versions of GYRO are planned to include a kinetic treatment of impurities (which are ignored in the present work), ion-ion collisions, compressional magnetic perturbations, and the so-called *parallel nonlinearity*.

Figure 2 summarizes a total of eight simulations (four at $\rho_* = 0.004$ and four at $\rho_* = 0.0026$) carried out to gauge the relative influence of various physical effects on transport. For each discharge and gyroradius, we show runs with (1) all physics, then with (2) no collisions, (3) no $\mathbf{E} \times \mathbf{B}$ equilibrium sheared rotation, and (4) zero β_e. Figures 2(a) and 2(b) show χ_i and χ_e, respectively. We can comment on the importance of various effects. First, electron collisions act to *reduce* the linear ion temperature gradient (ITG) growth rate (by reducing the trapped electron drive) thereby reducing the ion transport. This reduction is evident in both the electron and ion channels, in simulations at both values of ρ_*. Next, finite-β effects tend to stabilize ITG modes, and simultaneously destabilize KBM modes. For these discharges, β increases toward the core, and thus the modification to the transport is expected to be strongest there. In separate simulations we have observed that the β effect is essentially negligible at $r/a = 0.6$ (where $\beta \simeq 0.2\beta_{\text{crit}}$), but can reduce the transport by a factor of 2 in the vicinity of $r/a = 0.4$. This is borne out by the present simulations, which show a small finite-β effect (with a trend that is opposite for electrons and ions) at $r/a = 0.6$.

Finally, we find that $\mathbf{E} \times \mathbf{B}$, like collisions, gives rise to a substantial reduction in transport. This well-known effect is especially important for the DIII-D tokamak, but is expected to be somewhat reduced in importance for a reactor. It is worth noting that when run in flux-tube mode, GYRO gives $\chi_i/\chi_{\text{GB}} \simeq 10$, which is comparable to the small-ρ_* simulation without $\mathbf{E} \times \mathbf{B}$. This indicates that in the absence of $\mathbf{E} \times \mathbf{B}$, finite-$\rho_*$ effects are appreciable only for the large-ρ_* discharge. Conversely, if run in global mode but with adiabatic electrons, GYRO shows *zero* transport in the presence of $\mathbf{E} \times \mathbf{B}$.

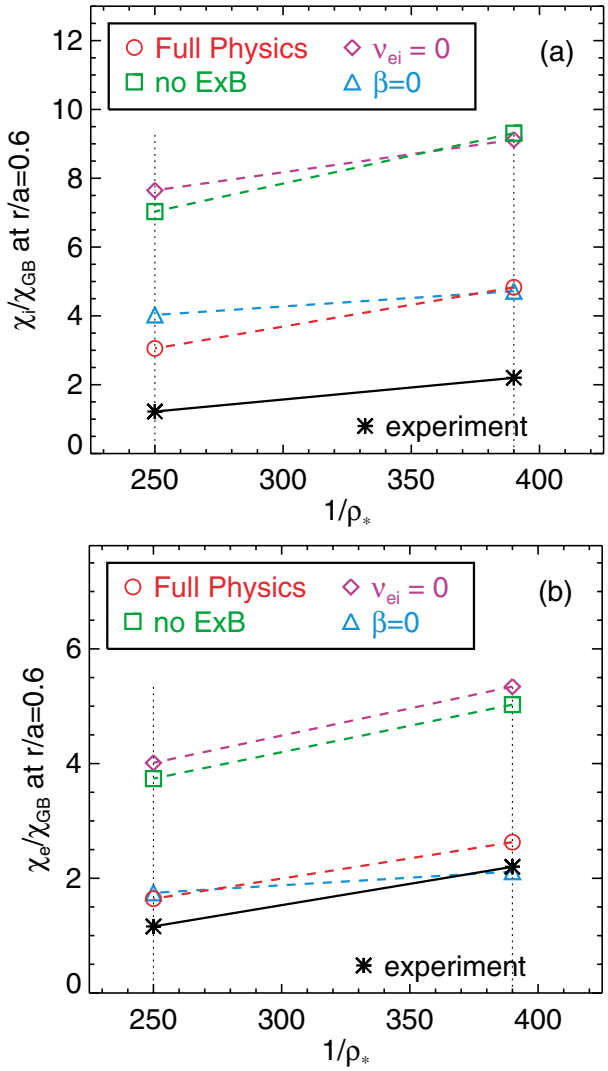

FIG. 2 (color online). Impact of selected physical effects on ion (a) and electron (b) energy transport, and comparison with experimental estimates.

The stiffness inherent in the transport problem is apparent from Fig. 3. Here, we find that the discrepancy between simulation (at baseline parameters) and experiment for shot 81 is about a factor of 2 in the ion channel. However, decreasing $-dT_i/dr$ by about 12% is enough to reduce χ_i and χ_e to experimental levels. This is particularly striking considering that the experimental uncertainty in $-dT_i/dr$ is estimated to be $\pm 30\%$. At $r_0/a = 0.6$ we are close to the threshold where the maximum linear growth rates just exceed the shear rate, so

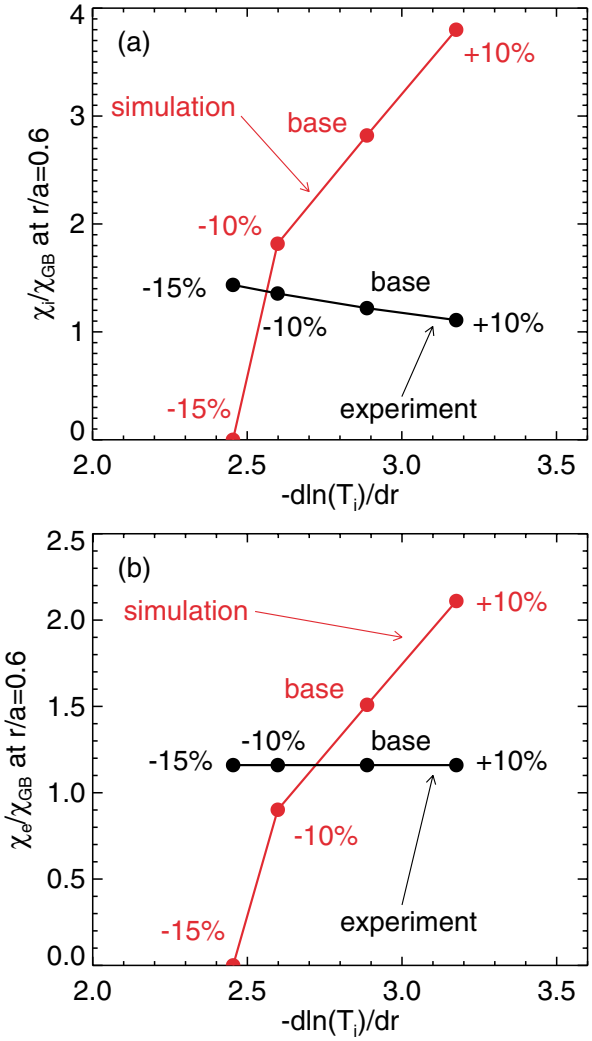

FIG. 3 (color online). Dependence of ion (a) and electron (b) transport on temperature gradient. Very close agreement in both electron and ion channel transport occurs for a 10% reduction in the baseline ion temperature gradient, whereas a 15% reduction eliminates transport entirely. Note that the actual experimental uncertainty in this gradient is estimated to be 30%.

that a small decrease in the growth rate has a big effect. This also explains the factor of 2 reduction in χ_i and χ_e (between Figs. 1 and 2) as m_i/m_e changes from 400 to 3600, even though the linear growth rates decrease by only about 15%. The core stiffness, with power flow very sensitive to R/L_T, was previously noted in Fig. 4 of [12].

Finally, we point out a remarkable feature of simulations with nonzero rotation. While rotation is evidently a major player in reducing the scaling from gyroBohm to Bohm, it also gives rise to a preferred direction of propagation of heat-flux avalanches, as shown in Fig. 4. For a fixed profile of rotation, these avalanches (of radially outward energy flux) propagate inward at a velocity

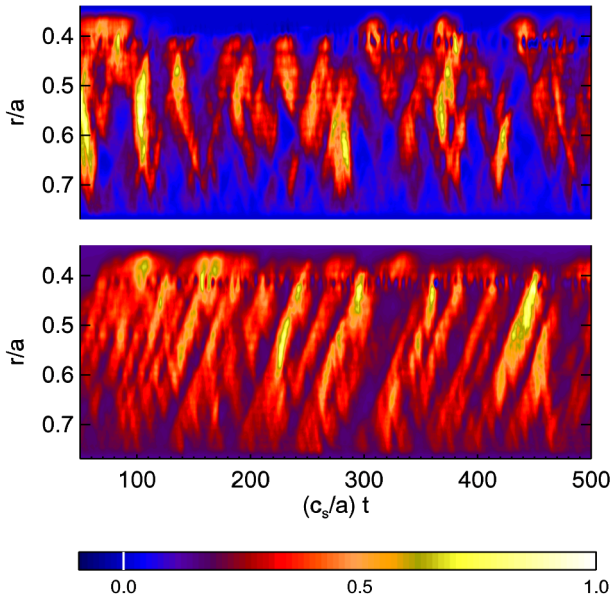

FIG. 4 (color online). Heat-flux avalanches induced by toroidal rotation. The upper frame shows the flux intensity (normalized) for a simulation with no toroidal rotation. When sheared rotation is switched on, avalanches of outward-directed heat-flux propagate inwards, as seen in the lower frame.

which decreases as ρ_* decreases. The intermittent nature of the flux at a fixed radius is also apparent.

This work was supported by U.S. DOE Grant NO. DE-FG03-95ER54309 and the SciDAC Plasma Microturbulence Project. We thank M. N. Rosenbluth and F. L. Hinton for their advice and insight and C. C. Petty for help with DIII-D data.

*Electronic address: http://web.gat.com/comp/parallel
[1] C. Petty *et al.*, Phys. Plasmas **2**, 2342 (1995).
[2] J. Candy and R. Waltz, J. Comput. Phys. **186**, 545 (2003).
[3] R. Sydora, V. Decyk, and J. Dawson, Plasma Phys. Controlled Fusion **38**, A281 (1996).
[4] S. E. Parker *et al.*, Phys. Plasmas **3**, 1959 (1996).
[5] Z. Lin *et al.*, Phys. Rev. Lett. **88**, 195004 (2002).
[6] F. Jenko and W. Dorland, Plasma Phys. Controlled Fusion **43**, A141 (2001).
[7] Y. Chen and S. Parker (private communication).
[8] S. E. Parker, C. Kim, and Y. Chen, Phys. Plasmas **6**, 1709 (1999).
[9] R. E. Waltz, J. Candy, and M. N. Rosenbluth, Phys. Plasmas **9**, 1938 (2002).
[10] L. Pareschi and G. Russo, in *Hyperbolic Problems: Theory, Numerics and Applications*, Proceedings of the 9th International Conference on Hyperbolic Problems, Pasadena, CA, 2002 (Springer-Verlag, Heidelberg, 2003).
[11] G. R. McKee *et al.*, Nucl. Fusion **41**, 1235 (2001).
[12] D. Ross and W. Dorland, Phys. Plasmas **9**, 5031 (2002).